Astronomy & Astrophysics manuscript no. main
October 7, 2014

Nickel mass estimates of Type Ia Supernovae from NIR data: Test case for heavily reddened objects

TBD

[1] European Southern Observatory, Karl Schwarzschild Strasse 2, Garching bei Munchen, Germany, 85748
e-mail: @eso.org
[2]

Preprint online version: October 7, 2014

Abstract

Aims. To determine the relation between the amount of radioactive Nickel (^{56}Ni) produced in Type Ia supernovae (SNIa) and the timing of the second maximum in the Near Infrared (NIR; YJH) bands and to extrapolate Nickel mass values for highly reddened SNIa using this relation
Methods. We measure the (pseudo)-bolometric luminosity at peak from the ultraviolet optical Near Infrared (UVOIR) light curves and use it to derive a value of $M_{^{56}Ni}$ mass for a 'low-reddening' sample of objects from the literature. These objects have low extinction from the host galaxy dust and hence, there are effects from presuming a reddening law are smaller.
Results. We find a strong correlation between the $M_{^{56}Ni}$ and t_2 in the Y and J bands and a weaker trend in the H band. We use this empirical relation to derive $M_{^{56}Ni}$ for test case SNae with high extinction. This allows us to have a $M_{^{56}Ni}$ value which is independent of the reddening law applied. We also apply the relation to all objects not in the low-reddening sample for which a t_2 is measured.
Conclusions. From our results we conclude that an empirical relation between $M_{^{56}Ni}$ and t_2 can allow us to infer the $M_{^{56}Ni}$ for highly reddened objects without an estimate of their total absorption. The results for SN2014J from this method correspond well with the values obtained from recent γ ray observations, thus providing further evidence of the potency of this technique

Key words. stars: supernovae: general

1. Introduction

Type Ia supernovae (SNe Ia) have been used as cosmological distance indicators and have provided first evidence for the accelerated expansion of the universe (Riess et al. 1998; Perlmutter et al. 1999). . Their potency as cosmological probes has led to dedicated efforts to understand the nature of these explosions to reduce effects from systematics in the constraints of the cosmological parameters.

SNIa in the optical, however, require corrections using correlations between observables (Phillips 1993; Tripp 1998) to improve cosmological parameter estimation. Recent studies of SNeIa have indicated that the SNIa are much more uniform in the NIR, which has led to systematic efforts in obtaining NIR light curves of Ia's. Another interesting feature of SNIa in the NIR is a second maximum that appears $\sim$ 15-35 days after maximum light in B-band. Kasen (2006) demonstrated that the second maximum could be the result of increased emissivity in the NIR due to the emergence of FeII/CoII lines at late times due to the cooling of the ejecta. This grid of models also showeds that larger iron mass would lead to a later maximum in the NIR light curves.

Recent studies have shown a strong dependence of the timing of the second maximum (hereafter t_2) on the decline rate of the SNIa, indicating that brighter explosions have a later onset of the second maximum. The models of Kasen & Woosley (2007) points towards a strong relation between $M_{^{56}Ni}$ and the reddening of the colour curve of an SNIa. A faster reddening of the optical colour curve would imply an earlier onset of the late-time uniform colour evolution (known, commonly, as the 'Lira Law'). A strong relation is observed between t_2 and the epoch of onset of the Lira law (t_L). The conclusions from these studies point to a connection between the $M_{^{56}Ni}$ in SNIa and t_2.

In this study, we investigate ,directly, the link between the $M_{^{56}Ni}$ and t_2. We use a sample of nearby objects with low extinction from host galaxy dust, in order to circumvent uncertainties from the specific reddening law used. We aim to use this relation to derive $M_{^{56}Ni}$ for heavily extinguished SNae where using the bolometric peak is extremely sensitive to the total absorption value used, and hence, the reddening law. To this end, we propose using NIR only data at late times along with an empirical relation to obtain precise estimates of $M_{^{56}Ni}$ for objects where other methods provide disparate results.

2. Data

The sample for this study is constrained by objects which have NIR observations at late times as well as well-sampled optical and NIR light curves to construct a (pseudo-) bolometric light curve. The main data source of near-infrared photometry of SNe Ia currently comes from the Carnegie Supernova Project (CSP; Contreras et al. 2010; **?**; Stritzinger et al. 2011; Phillips 2012; Burns et al. 2014). They form an ideal basis for an evaluation of light curves parameters. We add to this sample objects from the literature and the nearby objects eg. SN2011fe.

Since we aim to circumvent the uncertainties from host galaxy extinction, we only select objects with an $E(B-V)_{host}$

Send offprint requests to: TBD

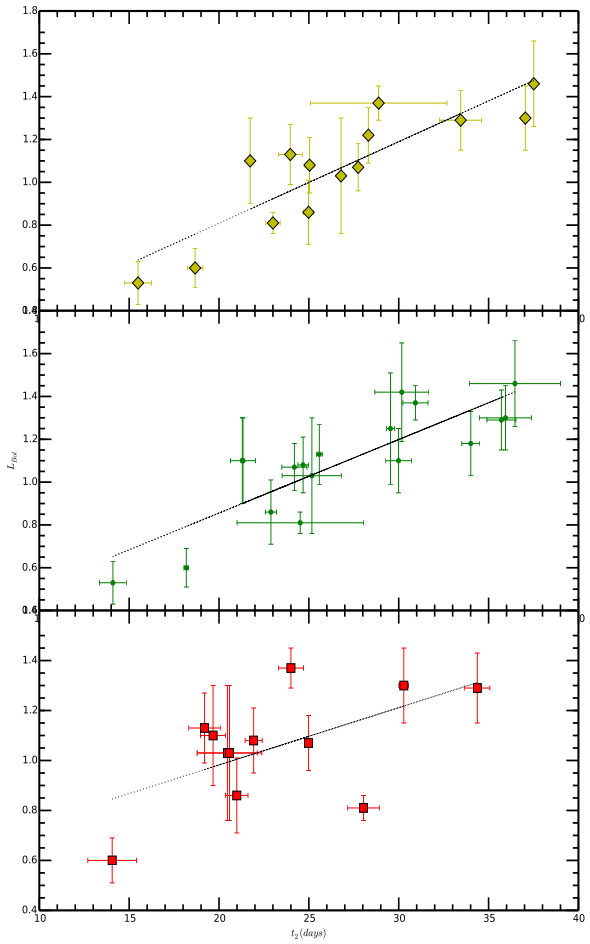

Figure 1. L_{max} is plotted against the t_2 in YJH bands. A strong correlation is observed in the Y and J, whereas a weaker correlation is seen in the H band. Best fit lines are overplotted in black.

value less than 0.1. The values for $E(B-V)_{host}$ are obtained from the literature, references for each object are given in 1. Since we want to investigate the connection of M_{Ni} with t_2 in the NIR, this excludes objects which are spectroscopically similar to the peculiar SN 1991bg (Filippenko et al. 1992; Leibundgut et al. 1993; Mazzali et al. 1997) and objects that do not exhibit a second maximum (SNe 2005bl, 2005ke, 2005ku, 2006bd, 2006mr, 2007N, 2007ax, SN2007ba, 2009F). On similar lines we exclude peculiar objects like 2006bt and 2006ot. For consistency, we also only include objects with coverage near maximum in u to H bands, and hence we do not need to apply corrections for missing passbands. These constraints leave us with a final sample of 19 objects.

3. Analysis

The flux emitted by an SNIa in the UV, optical and NIR traces the comptonization of the photons emitted through the ^{56}Ni $\rightarrow$ ^{56}Co $\rightarrow$ ^{56}Fe decay chain (see Nadyozhin 1994). As the SN emits most of its flux in the UV to NIR passbands, the "uvoir bolometric flux" represents a physically meaningful quantity (Suntzeff 1996)

We select a low-reddening sample so that our measurements are less sensitive to a reddening law. For objects with sufficient amount of near maximum data in the optical and the NIR, we construct UBVRIJH bolometric light curves. We do not use K band data since there are very few objects in the sample with well-sampled K band light curves. For objects with well-sampled K light curves we calculate the flux emitted in the K band and find that it is between $1-3\%$, thus, not using the K-band is not a dominant source of uncertainty. The magnitudes were corrected for reddening using a CCM reddening law for each filter. The values for the extinction are presented in table 2. The uncertainty in the reddening estimate was propagated into the calculation of the bolometric flux Using zero-points in the given filters, the magnitudes were converted to fluxes. The resulting light curve, in ergs/cm^2/s was converted into an absolute bolometric light curve by using the distances of the SN derived from the host galaxy redshift.

Since all distances are scaled to an $H_0 = 70 kms^{-1}Mpc^{-1}$the errors in the luminosity distance are only affected by the relative errors in the distance moduli (see Table 2 for values and uncertainty estimates). For objects not in the hubble flow, we use distance measurements from published estimates (which use others methods eg. Cepheid, Tully-Fisher relation etc.).

In our sample, for uniformity, we restrict the analysis to objects with coverage from $u-H$ bands with coverage around the bolometric peak.

Table 3. Values of the coefficients for correlations between L_{max} and t_2 in the individual filters

Filter	a_i	b_i
Y	0.045($\pm$0.005)	-0.150($\pm$0.140)
J	0.042($\pm$0.005)	-0.056($\pm$0.122)
H	0.039($\pm$0.010)	0.191($\pm$0.236)

4. Results

In this section we present the results derived from the measurements of the peak bolometric luminosity and the trends observed with other parameters for the SNe in our low-reddening sample. We also extend the analysis to the complete sample of objects with a measured second maximum.

4.1. Correlation between L_{max} and t_2

In figure 1, we find that there is a very strong correlation between t_2 and $M_{^{56}Ni}$ in the Y and J bands with r values of 0.80, 0.88. A much weaker trend is observed in the H band with $r \sim 0.60$. This is reflected in the ratio of the slope to the slope error in equation (**??**) In the Y and J band, a strong correlation suggests that objects with more Ni produced show later second maxima.

$$L_{max} = a_i \cdot t_2(i) + b_i \quad (1)$$

From Table 3 and figure 1, we can see that the constraints on the slope for the best fit relation in the H band are weak. Hence, for further analyses, we do not use the H band.

Equation (1) relates t_2 to the bolometric luminosity. The coefficients for the linear fit and the errors on the estimates are given in Table 3.

Table 1. The sample of SNe which have low reddening, as defined in the text. The references for the data are presented along with the extinction values and the distanes used to calculate the bolometric light curves

SN	μ	e_μ	$E(B-V)_{host}$	$E(B-V)_{MW}$	Filters	Reference	$t_2(J)$	$t_2(Y)$ [a]
SN2001ba	35.40	0.50	0.010(0.04)	0.021 (0.002)	UBVRIJH	K04a	34.01 ± 0.90	...
SN2002dj	31.70	0.30	0.020(0.03)	0.080 (0.003)	UBVRIJH	P08	31.14 ± 1.83	...
SN2002fk	32.59	0.15	0.030(0.01)	0.030 (0.003)	UBVRIJH	C14	29.54 ± 0.23	...
SN2005M	35.01	0.09	0.060(0.021)	0.027(0.002)	UBVRIJH	B14	30.93 ± 0.70	28.88 ± 3.80
SN2005am	32.85	0.20	0.053(0.017)	0.043(0.002)	UBVRIJH	B14	21.34 ± 0.70	21.73 ± 0.12
SN2005el	34.04	0.14	0.015(0.012)	0.098 (0.001)	UBVRIJH	B14	24.64 ± 0.64	24.96 ± 0.11
SN2005eq	35.46	0.07	0.044(0.024)	0.063(0.003)	UBVRIJH	B14	35.00 ± 0.70	37.48 ± 0.12
SN2005hc	36.50	0.05	0.049(0.019)	0.028(0.001)	UBVRIJH	B14	36.47 ± 2.54	37.51 ± 0.10
SN2005iq	35.80	0.15	0.040(0.015)	0.019(0.001)	UBVRIJH	B14	24.19 ± 0.70	27.74 ± 0.05
SN2005ki	34.73	0.10	0.016(0.013)	0.027(0.001)	UBVRIJH	B14	25.17 ± 1.66	26.79 ± 0.06
SN2006bh	33.28	0.20	0.037(0.013)	0.023(0.001)	UBVRIJH	B14	22.89 ± 0.31	24.98 ± 0.28
SN2007bd	35.73	0.07	0.058(0.022)	0.029(0.001)	UBVRIJH	B14	...	28.31 ± 0.11
SN2007on	31.45	0.08	< 0.007	0.010(0.001)	UBVRIJH	B14	18.18 ± 0.13	18.67 ± 0.43
SN2008R	33.73	0.16	0.009(0.013)	0.062(0.001)	UBVRIJH	B14	14.10 ± 0.74	15.49 ± 0.74
SN2008bc	34.16	0.13	< 0.019	0.225(0.004)	UBVRIJH	B14	33.33 ± 0.23	32.90 ± 0.32
SN2008gp	35.79	0.06	0.098(0.022)	0.104(0.005)	UBVRIJH	B14	35.71 ± 0.81	33.45 ± 1.17
SN2008hv	33.84	0.15	0.074(0.023)	0.028(0.001)	UBVRIJH	B14	24.68 ± 0.29	25.04 ± 0.25
SN2008ia	34.96	0.09	0.066(0.016)	0.195(0.005)	UBVRIJH	B14	25.58 ± 0.16	23.97 ± 0.67
SN2011fe	28.91	0.20	0.014(0.01)	0.021(0.001)	UBVRIJH	Pa13 29.99 ± 0.79	...	

[a] E(B-V) references, K04a: Krisciunas et al. (2004);
P08: Pignata et al. (2008); C14: Cartier et al. (2014)
B14:Burns et al. (2014); Pa13: Patat et al. (2013)

Table 2. L_{max} measurements for low reddening SNIa with a measured t_2.

SN	$L_{max}(\cdot e^{43} ergs^{-1})$	e_L	$M_{Ni} - Arn(M_\odot)$	$M_{Ni} - Arn(M_\odot)$ (fixed rise)	$M_{Ni} - DDC(M_\odot)$
SN2001ba	1.18	0.15	0.58	0.59	0.57
SN2002dj	1.25	0.26	0.59	0.63	0.61
SN2002fk	1.42	0.23	0.68	0.71	0.76
SN2005M	1.37	0.08	0.70	0.69	0.71
SN2005am	1.1	0.2	0.47	0.55	0.52
SN2005el	0.91	0.11	0.40	0.46	0.44
SN2005eq	1.32	0.2	0.67	0.66	0.67
SN2005hc	1.46	0.2	0.74	0.73	0.79
SN2005iq	1.07	0.11	0.48	0.54	0.51
SN2005ki	1.03	0.27	0.45	0.51	0.49
SN2006bh	0.86	0.15	0.37	0.43	0.40
SN2007bd	1.22	0.13	0.55	0.61	0.59
SN2007on	0.6	0.09	0.24	0.30	0.28
SN2008R	0.53	0.1	0.21	0.26	0.25
SN2008bc	1.32	0.19	0.63	0.66	0.67
SN2008gp	1.29	0.14	0.62	0.65	0.64
SN2008hv	1.08	0.13	0.48	0.54	0.52
SN2008ia	1.13	0.14	0.50	0.56	0.55
SN2011fe	1.1	0.15	0.50	0.50	0.52

4.2. Low galactic reddening sample

In our sample, we selected objects with a host galaxy extinction < 0.1 mag. For some of these objects, the galactic extinction is > 0.1 mag. In order to see whether these objects influence the strength of the correlation, we evaluate the correlation coefficients for a sample without the high galactic reddening objects. As a result, 7 objects with $E(B-V)_{host}$ <0.1 but total E(B-V) ≥ 0.1 are removed. We do not find a substantial decrease in the correlation coefficients in the YJH bands, which are 0.76, 0.83, 0.60 respectively. Since we know the reddening law in the MW with high certainty, we can correct the bolometric light curves for the absorption from the MW dust. Thus, for further analysis we do not truncate the sample from the original low reddening objects in Table 1

4.3. Deriving $M_{^{56}Ni}$ from L_{max}

In the sections above, we have found a strong correlation between the peak bolometric luminosity (L_{max}) and t_2 in the Y and J bands.

Since our final aim is to derive a value of the ^{56}Ni mass for objects which have a measured value of t_2, we present the different methods to derive $M_{^{56}Ni}$ from the peak bolometric luminosity.

In figure 4, we plot the distributions of the $M_{^{56}Ni}$ from the different methods.

4.3.1. Arnett's rule with a variable rise time

Arnett's rule states that the luminosity of the SN at peak is given by the instantaneous rate of energy deposition from radioactive decays inside the expanding ejecta. This is summarized in equation (**??**).

$$L_{max} = \alpha E_{Ni}(t_R) \quad (2)$$

Where E_{Ni} is the input from ^{56}Ni decay at maximum, t_R is the rise time and α accounts for deviations from Arnett's Rule.

$$E_{Ni}(1M_\odot) = 6.45 \cdot 10^{43} e^{-t_R/8.8} + 1.45 \cdot 10^{43} e^{-t_R/111.3} \quad (3)$$

For estimates using different rise times, we follow the relation in **?**

$$t_{R,B} = 17.5 - 5(\Delta m_{15} - 1.1) \quad (4)$$

and

$$t_{R,Bol} = t_{R,B} + (t_{max,bol} - t_{max,B}) \quad (5)$$

which implies

$$L_{max} = \alpha \cdot (6.45 \cdot 10^{43} e^{-(t_{R,bol}/8.8)} + 1.45 \cdot 10^{43} e^{-t_{R,bol}/111.3}) \cdot (M_{Ni}/M_\odot) \quad (6)$$

substituting the relation derived between L_{max} and t_2 (equation (1)) we get a relation between t_2 and $M_{^{56}Ni}$

$$M_{Ni} = \frac{a_i \cdot t_2(i) + b_i}{\alpha \cdot E_{Ni}(t_2(i))} \quad (7)$$

From equation (7), we can see that the relation between $M_{^{56}Ni}$ and t_2 is non-linear.

4.3.2. Arnett's rule with a fixed rise time

For this method of deriving $M_{^{56}Ni}$ from L_{max}, we use a fixed rise time of 19 days, as in Stritzinger et al. (2006). Similar to their analysis, we propagate an uncertainty of $\pm$ 3 days

$$L_{max} = (2.0 \pm 0.3) \cdot 10^{43} (M_{Ni}/M_\odot) ergs^{-1} \quad (8)$$

For deriving equation (8) we need to use a specific value of α. In previous studies (eg. Stritzinger et al. 2006; Mazzali et al. 2007), the authors use α=1. This value is very close to the self consisent models of Arnett (1982) and is also the mean values for the models of Höflich, Khokhlov & Wheeler (1995). Hence, in our study, we use α=1.

From the DDC models, we calculate the ratio of decay energy to the bolometric luminosity (which is the α value) for the different $M_{^{56}Ni}$ input values. We find that the values have a mean of 1.03 with a σ of 0.07. We find that these values are consistent with the simplifying assumption that α=1.

4.3.3. Interpolating using DDC models

Another possible method for deriving $M_{^{56}Ni}$ values from L_{bol} is by interpolating the relation found from theoretical models between these two quantities. In our analysis, we use the DDC models from Blondin et al. (2013) as another method of obtaining $M_{^{56}Ni}$.

For objects without NIR coverage, these models can be used to calculate the $M_{^{56}Ni}$-L_{Bol} relationship for a set of optical-only filters (eg. SN2004gu only has $BVRI$ coverage near maximum).

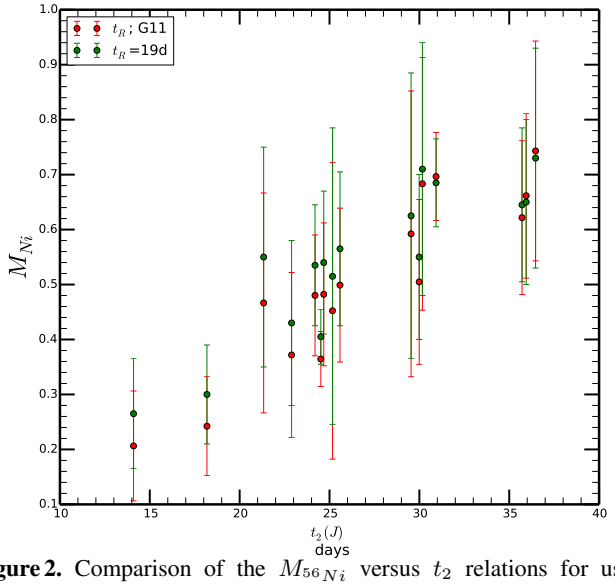

Figure 2. Comparison of the $M_{^{56}Ni}$ versus t_2 relations for using Arnett's rule with variable (*red circles*) and fixed (*green circles*) rise time.

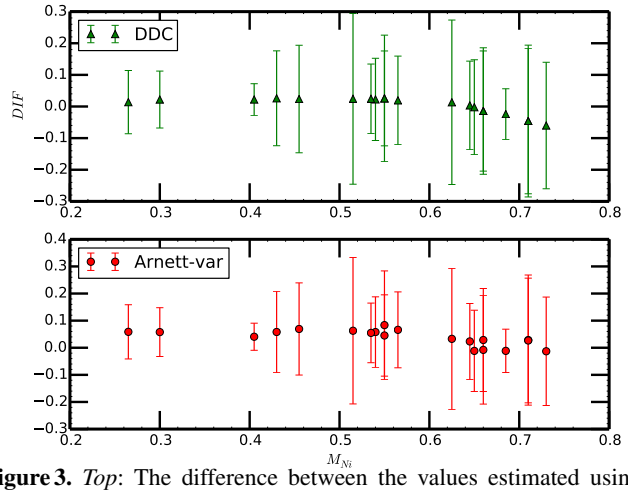

Figure 3. *Top*: The difference between the values estimated using a fixed rise time with Arnett's rule and the DDC models is plotted against the estimates from Arnett's rule with fixed rise time. *Bottom*: The difference between values estimated using a fixed rise time with Arnett's rule and a variable rise time plotted against the estimates from Arnett's rule with fixed rise time. From the two panels we can see that the difference in the individual measurements are much smaller than the errors from a given method

This method, therefore, has the advantage of being able to derive $M_{^{56}Ni}$ values for objects with missing passbands without an additional correction term applied to the bolometric luminosity. However, in order to keep the samples uniform across the different methods, we only use the objects with complete coverage from u ot H bands.

Similar to previous studies we find that there is a large distribution in the $M_{^{56}Ni}$ values for the sample in Table 1. We note a factor of $\sim$ 3 difference between the lowest and highest $M_{^{56}Ni}$ values. We note that this sample doesn't include faint, 91bg-like objects, since their NIR light curves don't show a second maximum. These objects are seen to have a much lower $M_{^{56}Ni} \sim$ 0.1 $M_\odot$. Thus, the complete distribution of $M_{^{56}Ni}$ for SNIa is expected to be wider than is seen in our sample.

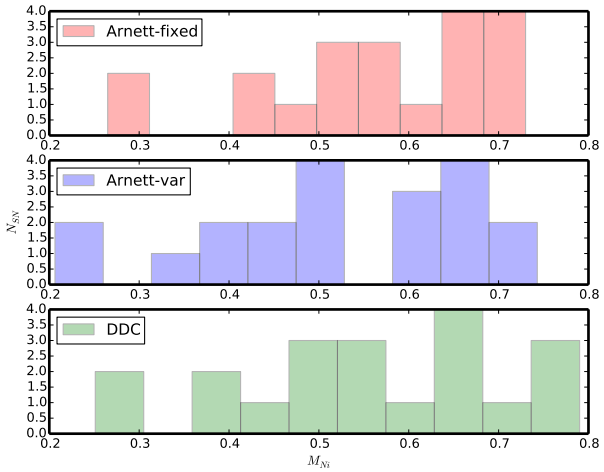

Figure 4. The histograms show the different methods to estimate the M_{56Ni} from the L_{max}. The values from Arnett's rule with fixed and variable rise time are plotted in the *top* and *middle* panels. The *bottom* panel has the values estimated from the DDC models

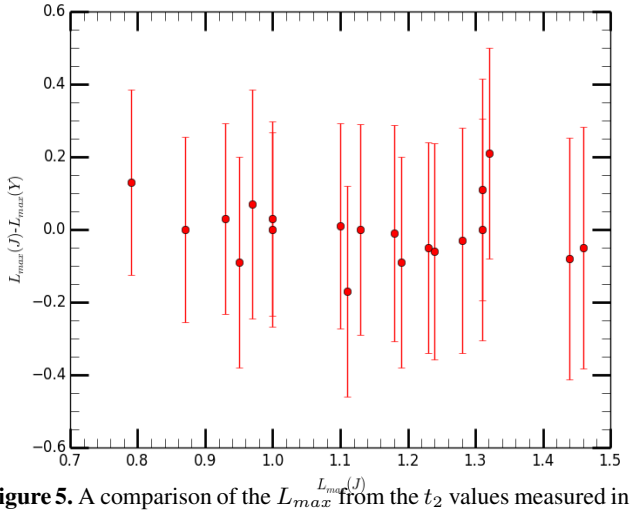

Figure 5. A comparison of the L_{max} from the t_2 values measured in the Y and J bands. Plotted on the x-axis is the L_{max} measured from $t_2(J)$ and on the y-axis is the difference between $L_{max}(J)$ and $L_{max}(Y)$. We can see that there is no trend between the two. The difference has a standard deviation of 0.08 ($\cdot$ $1e^{43}$) $ergs^{-1}$. The errors on each are errors in the individual measurements added in quadrature. We can see that the difference is smaller than the error.

4.4. Test Case for heavily reddened SNe

Using the correlations derived above, we want to estimate the Ni masses of heavily reddened SNae. The first test case is the nearby SN 2014J in M82 with an $E(B-V)_{host}$ of 1.3. Current attempts to use the bolometric light curve depend on the A_V value used and vary by a factor of ~ 2 (0.37 $M_\odot$ if using A_V=1.7 mag from Margutti et al. (2014), compared to 0.77 using a higher A_V of 2.5 mag from Goobar et al. (2014)). In our analyses the aim is to estimate the M_{56Ni} independent of the extinction.

The proximity of SN2014J, has allowed for the first γ ray Co line detection in an SNIa (Churazov+ 2014). the authors, using a line photon escape fraction from the models, deduce an Ni mass of 0.62 ± 0.13 $M_\odot$. This provides a direct measurement of M_{Ni} for the SN. However, γ ray detections aren't possible for farther away SN, for which we require a different estimation method.

Using the best fit relation for the sample defined above , we obtain M_{56Ni} of 0.66 ± 0.15 $M_\odot$ for a t_2 of 31.99 ± 1.15 days. Thus, we find a very good correspondence between the values from the γ rays and the NIR second maximum. This adds evidence to the argument that the NIR can be used for estimate M_{56Ni} for highly reddened SN.

Since we find from the DDC models that α is not constant for different M_{56Ni} (and hence, L_{max}) values, we use α corresponding to the peak luminosity of SN2014J. We do not find a significant change in the estimated M_{56Ni}. Hence, for further analyses, we use α=1

For SN2014J, we can get a precise measurement of the extinction from IR spectra at $\sim$ +300 days (**explain in greater detail**). This is again not possible for objects farther away. Thus, we apply this relation to a farther away, heavily extinguished object, SN2006X. The measured value for SN2006X of $t_2(J)$ is 28.19 with an error of 0.49 days. This results in an M_{56Ni} value of 0.58 ± 0.13 $M_\odot$. This value is consistent with the conclusion that SN2006X is a 'normal' SNIa (Wang et al. 2008). We compare this value for SN2006X to that obtained using $t_2(Y)$ and obtain M_{56Ni} of 0.58 ± 0.14 $M_\odot$. We find both these values consistent with each other. The slightly higher error bar on the value from $t_2(Y)$ is due to a larger error on the intercept in the best fit relation for the Y band.

In Wang et al. (2008), the authors use multi-band photometry to correct the light curves for absorption from host galaxy dust. They derive a bolometric peak luminosity of 1.02 ($\pm$ 0.1) $\cdot e43$ $ergs^{-1}$. From R band photometry, they derive a rise time to B maximum of 18.2 ± 0.9d. Using this value in the expression for Arnett's rule, they derive a value of M_{56Ni}= 0.50 ± 0.05 $M_\odot$. Thus, we conclude that the value derived from t_2 is consistent with published M_{Ni} values.

We include three more objects in the highly reddened SNe sample, namely, 1986G, 2005A and 2008fp. We calculate the M_{56Ni} for these objects in the same way as for SN2014J and SN2006X. We summarise our findings in Table 5. We can see that 1986G has a lower value of M_{56Ni} than the other objects in the sample. This is consistent with the observed optical decline rate and lower B band luminosity of the SN. Since we find that t_2 in both Y and J bands correlates very strongly with the M_{56Ni}, we use combined constraints from the relations to obtain an M_{56Ni} estimate. We can see from Table 5 that the error on the M_{56Ni} reduces when using combined constraints. For 2014J, it is 0.17 $M_\odot$ whereas for the others it is much lower at 0.07 $M_\odot$

Hence, we conclude that the NIR second maximum timing (in Y and J) is a very good indicator of the amount of Nickel synthesised in the explosion, even for heavily reddened objects.

4.5. Complete NIR Sample

Since we have derived the relation between L_{max} and t_2, we evaluate the L_{max} for all objects with a measured t_2 independent of the reddening estimates. Since the slope for the relation in the Y and J bands is very similar and the intercepts are within error bars, we take the mean value for the slope and intercept as a 'combined' relation. We use the higher error on the intercept (from the Y band) for the combined equation. We then use this to compare the estimates of L_{max} from the t_2 in the two bands. In figure 5, we plot the difference in the L_{max} from the t_2 in J and Y against the L_{max} estimated from $t_2(J)$. The difference in the two estimates is smaller than the error on the measurement. We note that the largest difference is for SN2005na, which has a $t_2(J)$ of 32.59, but a much smaller $t_2(Y)$ of 27.54. However, even for this object, the error is higher than the difference between the measurements

Table 4. Comparison of different methods to estimate $M_{^{56}Ni}$ for SN2014J

M_{Ni} (inferred)	σ	Method	Reference
0.62	0.13	γ ray lines	Churazov et al. (2014)
0.37	–	Bolometric light curve A_V=1.7 mag	Churazov et al. (2014); Margutti et al. (2014)
0.77	–	Bolometric light curve A_V=2.5 mag	Churazov et al. (2014); Goobar et al. (2014)
0.64	0.12	NIR second maximum	this work

Table 5. M_{Ni} estimates for 5 objects with high values of $E(B-V)_{host}$. We present constraints from the relation using only $t_2(J)$ as well as from both $t_2(Y)$ and $t_2(J)$. We can see a marked decrease in the error values when combined constraints are used

SN	$t_2(J)$	M_{Ni} (inferred)	σ	μ	e_μ	Method
SN1986G	16.40 ($\pm$ 1.4)	0.32	0.10	28.01	0.12	J band relation
–	–	0.33	0.08	–	–	combined fit
SN2005A	27.58 ($\pm$ 0.3)	0.57	0.13	34.51	0.11	J band relation
–	–	0.57	0.11	–	–	combined fit
SN2006X	28.19 ($\pm$ 0.5)	0.57	0.13	30.91	0.08	J band relation
–	–	0.58	0.11	–	–	combined fit
SN2008fp	31.03 ($\pm$ 0.3)	0.64	0.15	31.79	0.05	J band relation
– -	–	0.64	0.13	–	–	cf
SN2014J	31.99 ($\pm$ 1.2)	0.66	0.15	27.64	0.10	J band relation
–	–	0.66	0.13	–	–	combined fit

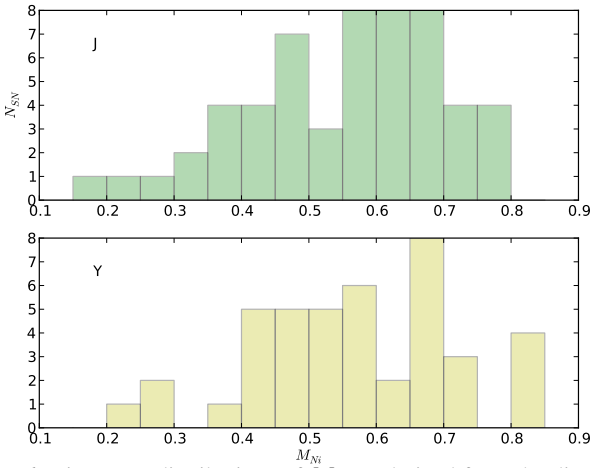

Figure 6. Histogram distributions of $M_{^{56}Ni}$ derived from the distributions of t_2 for a complete sample of SNIa with measured t_2. This uses the Arnett's rule derivation with fixed rise time.

In section 4.3, we have described the different methods for obtaining $M_{^{56}Ni}$ from L_{max}. Hence, we can derive a distribution for $M_{^{56}Ni}$ from the evaluated L_{max} for the complete sample.

In figure 6 we plot the distribution of $M_{^{56}Ni}$ calculated from the L_{max}. We use Arnett's rule with a fixed rise time to get the $M_{^{56}Ni}$ from the L_{max}. From figure 6, we find a large scatter in the $M_{^{56}Ni}$ values. We find that the objects vary by a factor of 3 in their $M_{^{56}Ni}$ distribution. We note, however, that since faint, 91bg-like objects do not show a second maximum, we do not have values in the figure $\lesssim$ 0.2 $M_\odot$, hence, the expected variation for the complete population of SNIa is greater.

In table **??**, we present the $M_{^{56}Ni}$ values for the complete sample of objects with a measured $t_2(J)$ value.

In figure 5, we plot the difference between the L_{max} estimated from the t_2 in Y and J bands against the L_{max} estimated from $t_2(J)$ (called $L_{max}(J)$ in the figure). We find that there is no relation between the two quantities. The mean difference is 0.002 $M_\odot$ with a standard deviation of 0.08 $M_\odot$. This is lower than the error estimate on the individual values, which can be seen in the figure.

4.6. Comparison with published values

We searched the literature for published values of $M_{^{56}Ni}$ for objects in our sample. In Scalzo et al. (2014) , the authors published values of $M_{^{56}Ni}$ for 2005el and 2011fe. For 2011fe, we find $M_{^{56}Ni}$ of 0.52 $\pm$ 0.15 $M_\odot$ whereas the value in S14 is 0.42 $\pm$ 0.08. We note that the value of α in their study is 1.2 whereas we use α=1. Using their value of α, we find $M_{^{56}Ni}$= 0.44 $M_\odot$, which is a better agreement.

For SN2005el we find $M_{^{56}Ni}$ of 0.46 $\pm$ 0.11 $M_\odot$. S14 provides a discussion of this object, which in their sample they measure to have an M_{Ni} of 0.52. It is one of two outliers in their $M_{^{56}Ni}$-Δm_{15}. They argue that it is likely for the SN to have a lower $M_{^{56}Ni}$ that their fiducial analysis suggests.

5. Discussion and Conclusion

In our sample, we observe a strong correlation between the L_{max} and t_2 in Y and J, and a weaker trend in the H band. This provides us with direct evidence that the timing of the second maximum is governed by the amount of Nickel produced by the supernova since it leads to a later ionization transition of the iron group elements at late time (mainly, ^{56}Co) from doubly to singly ionized (Kasen 2006).

This relation offers great insight into measuring the $M_{^{56}Ni}$ for objects not in the low-reddening sample, but with extensive NIR data. We compare different methods to obtain the $M_{^{56}Ni}$ from the L_{max} and find that they yield consistent estimates. The α parameter, which encodes the deviation from Arnett's, is chosen to be 1. We find that the DDC models show a very small deviation from this value for the grid of input $M_{^{56}Ni}$. We find that varying the α according to the models doesn't change the estimated $M_{^{56}Ni}$ and hence, for our analyses, we keep α as 1 when using Arnett's rule.

An example of an application of this method is the nearby SN2014J in M82, which is heavily occluded by host galaxy dust.

Table 6. M_{Ni} measurements for the complete sample of objects with t_2 measurements in both Y and J bands.

SN	$M^a_{^{56}Ni}$ (J)	σ	$M^a_{^{56}Ni}$ (Y)	σ
1980N	0.45	0.13		
1981B	0.67	0.15		
1986G	0.32	0.09		
1998bu	0.62	0.14		
1999ac	0.55	0.14		
1999ee	0.72	0.16		
2000E	0.67	0.16		
2000bh	0.68	0.15		
2001bt	0.58	0.13		
2001cn	0.62	0.14		
2001cz	0.71	0.16		
2001el	0.64	0.15		
2002bo	0.59	0.13		
2003cg	0.62	0.14		
2003hv	0.45	0.12		
2004ey	0.55972	0.18827	0.60606	0.20078
2004gs	0.41960	0.16062	0.42107	0.16925
2004gu	0.69188	0.22776	0.71609	0.22037
2005A	0.52479	0.18464	0.52129	0.18149
2005al	0.47613	0.18247	0.48234	0.17790
2005na	0.63129	0.20410	0.51847	0.19134
2006D	0.48280	0.18409	0.46976	0.17538
2006X	0.54244	0.18385	0.54012	0.18786
2006ax	0.61693	0.20145	0.62951	0.20647
2006gt	0.41	0.11		
2006et	0.62377	0.21597	0.62562	0.20453
2006hb	0.38320	0.17574	0.32494	0.15151
2006kf	0.45352	0.17771	0.49185	0.19541
2007S	0.68068	0.21642	0.72577	0.23435
2007af	0.56375	0.19466	0.57156	0.19483
2007as	0.46589	0.22175	0.43634	0.17288
2007bm	0.52969	0.17733	0.60822	0.20281
2007le	0.58617	0.19980	0.60800	0.19635
2007nq	0.45044	0.18491	0.43375	0.16546
2008C	0.62455	0.21035	0.56493	0.18960
2008fp	0.59200	0.20136	0.62030	0.20927
2014J	0.66	0.15		

[a]:$M_\odot$

Since this prevents an accurate measurement of $M_{^{56}Ni}$ from the bolometric light curves and there is a large disparity in the different values published in the literature using this method, we use the relations we obtain to constrain the $M_{^{56}Ni}$. For SN2014J, we have a unique opportunity to compare different estimation methods, since its proximity has allowed γ ray Co line detection and therefore, another extinction independent measurement of the $M_{^{56}Ni}$. Our value of 0.66 $\pm$ 0.15 $M_\odot$ compares very well with Churazov et al. (2014), who find $M_{^{56}Ni}$ of 0.61 $\pm$ 0.13 $M_\odot$. The brightness of SN2014J at late times, due to its proximity, permits us to obtain NIR spectra at $\sim$ 300 days, which can provide an accurate measurement of the extinction and therefore, an accurate $M_{^{56}Ni}$ from the bolometric light curve. This presents us with a confrontation of several different methods to measure the $M_{^{56}Ni}$ and hence obtain a conclusive estimate on the amount of Ni produce in this SN.

The recent discovery of ^{56}Ni in the outer layers of the ejecta of SN2014J (Diehl et al. 2014) offers insight into the nature of the ejecta structure. Our analysis cannot account for the Ni in the outer layers and therefore, the total amount of ^{56}Ni produced would be greater than the value of 0.66 $M_\odot$ we have obtained. In (Diehl et al. 2014) the authors have measured the $^{56}M_{Ni}$ from the γ ray emission of ^{56}Co at 847 and 1238 keV. From two different methods they obtain ranges of 0.42-0.56 ($\pm$ 0.06 $M_\odot$) and 0.52-0.59 ($\pm$ 0.13 $M_\odot$). These values are broadly consistent with our finding of 0.66 $\pm$ 0.15 $M_\odot$ and with the estimates summarized in Table 4.4

Since γ detections are unlikely for farther out SN and most of them are too faint at $\sim$ +300 days for IR spectroscopy, we apply our method to other heavily reddened SN that are farther away than SN2014J. The first object we analyse is SN2006X. From the measurement of 0.58 $\pm$ 0.13 $M_\odot$, we conclude that 2006X produced the average amount of Ni for an SNIa. We compare this value to the analysis in Wang et al. (2008), where the authors use multi-band light curves to obtain an A_V value and then calculate the bolometric luminosity from which they derive the $M_{^{56}Ni}$ using Arnett's rule. Their final value of 0.5 $\pm$ 0.05 $M_\odot$ is consistent with the value we obtain from the NIR light curve. **needs completion**

References

Ajhar E. A., Tonry J. L., Blakeslee J. P., Riess A. G., Schmidt B. P., 2001, ApJ, 559, 584
Amanullah R., et al., 2014, ApJ, 788, 21
Arnett W. D., 1982, ApJ, 253, 785
Benetti S., et al., 2004, MNRAS, 348, 261
Biscardi I., et al., 2012, A&A, 537, A57
Blondin S., Dessart L., Hillier D. J., Khokhlov A. M., 2013, MNRAS, 429, 2127
Branch D., Tammann G. A., 1992, ARA&A, 30, 359
Burns C. R., et al., 2014, ApJ, 789, 32
Cardelli J. A., Clayton G. C., Mathis J. S., 1989, ApJ, 345, 245
Cartier R., et al., 2014, ApJ, 789, 89
Churazov E., et al., 2014, Natur, 512, 406
Contardo G., Leibundgut B., Vacca W. D., 2000, A&A, 359, 876
Contreras C., et al., 2010, AJ, 139, 519
Diehl R., et al., 2014, arXiv, arXiv:1407.3061
Diehl R., et al., 2014, arXiv, arXiv:1409.5477
Filippenko A. V., et al., 1992, AJ, 104, 1543
Folatelli G., et al., 2010, AJ, 139, 120
Foley R., et al., 2014, arXiv, arXiv:1405.3677
Freedman W. L., et al., 2001, ApJ, 553, 47
Friedman A. S., et al., 2014, arXiv, arXiv:1408.0465
Ganeshalingam M., Li W., Filippenko A. V., 2011, MNRAS, 416, 2607
Goobar A., Leibundgut B., 2011, ARNPS, 61, 251
Goobar A., et al., 2014, ApJ, 784, L12
Hillebrandt W., Niemeyer J. C., 2000, ARA&A, 38, 191
Höflich P., Khokhlov A., Wheeler C., 1995, ASPC, 73, 441
Jack D., Hauschildt P. H., Baron E., 2012, A&A, 538, A132
Jensen J. B., Tonry J. L., Barris B. J., Thompson R. I., Liu M. C., Rieke M. J., Ajhar E. A., Blakeslee J. P., 2003, ApJ, 583, 712
Jha S., Riess A. G., Kirshner R. P., 2007, ApJ, 659, 122
Kasen D., 2006, ApJ, 649, 939
Kasen D., Woosley S. E., 2007, ApJ, 656, 661
Kattner S., et al., 2012, PASP, 124, 114
Krisciunas K., et al., 2001, AJ, 122, 1616
Krisciunas K., et al., 2003, AJ, 125, 166
Krisciunas K., et al., 2004a, AJ, 127, 1664
Krisciunas K., et al., 2004b, AJ, 128, 3034
Krisciunas K., et al., 2007, AJ, 133, 58
Krisciunas K., et al., 2009, AJ, 138, 1584
Kromer M., Sim S. A., 2009, MNRAS, 398, 1809
Leaman J., Li W., Chornock R., Filippenko A. V., 2011, MNRAS, 412, 1419
Leibundgut B., 1988, PhD thesis, University of Basel
Leibundgut B., 2000, A&ARv, 10, 179
Leibundgut B., 2001, ARA&A, 39, 67
Leibundgut B., et al., 1993, AJ, 105, 301
Leloudas G., et al., 2009, A&A, 505, 265
Li W., et al., 2001, PASP, 113, 1178
Li W., et al., 2003, PASP, 115, 453
Lira P., 1996, MsT, 3
Maeda K., Taubenberger S., Sollerman J., Mazzali P. A., Leloudas G., Nomoto K., Motohara K., 2010, ApJ, 708, 1703
Maeda K., et al., 2011, MNRAS, 413, 3075
Maguire K., et al., 2012, MNRAS, 426, 2359

Marion G. H., Höflich P., Gerardy C. L., Vacca W. D., Wheeler J. C., Robinson E. L., 2009, AJ, 138, 727
Mandel K. S., Wood-Vasey W. M., Friedman A. S., Kirshner R. P., 2009, ApJ, 704, 629
Margutti R., Parrent J., Kamble A., Soderberg A. M., Foley R. J., Milisavljevic D., Drout M. R., Kirshner R., 2014, ApJ, 790, 52
Mazzali P. A., Chugai N., Turatto M., Lucy L. B., Danziger I. J., Cappellaro E., della Valle M., Benetti S., 1997, MNRAS, 284, 151
Mazzali P. A., Cappellaro E., Danziger I. J., Turatto M., Benetti S., 1998, ApJ, 499, L49
Mazzali P. A., Röpke F. K., Benetti S., Hillebrandt W., 2007, Sci, 315, 825
Matheson T., et al., 2012, ApJ, 754, 19
Meikle W. P. S., 2000, MNRAS, 314, 782
Nadyozhin D. K., 1994, ApJS, 92, 527
Nobili S., et al., 2005, A&A, 437, 789
Nobili S., Goobar A., 2008, A&A, 487, 19
Pastorello A., et al., 2007, MNRAS, 377, 1531
Patat F., et al., 2013, A&A, 549, A62
Perlmutter S., et al., 1999, ApJ, 517, 565
Phillips M. M., 1993, ApJ, 413, L105
Phillips M. M., 2012, PASA, 29, 434
Phillips M. M., Lira P., Suntzeff N. B., Schommer R. A., Hamuy M., Maza J., 1999, AJ, 118, 1766
Phillips M. M., et al., 2006, AJ, 131, 2615
Phillips M. M., et al., 2013, ApJ, 779, 38
Pignata G., et al., 2008, MNRAS, 388, 971
Pinto P. A., Eastman R. G., 2000, ApJ, 530, 757
Riess A. G., Press W. H., Kirshner R. P., 1996, ApJ, 473, 88
Riess A. G., et al., 1998, AJ, 116, 1009
Scalzo R., et al., 2010, ApJ, 713, 1073
Scalzo R., et al., 2012, ApJ, 757, 12
Scalzo R., et al., 2014, MNRAS, 560
Stritzinger M., Leibundgut B., Walch S., Contardo G., 2006, A&A, 450, 241
Stritzinger M. D., et al., 2011, AJ, 142, 156
Suntzeff N. B., 1996, ssr..conf, 41
Tonry J. L., Dressler A., Blakeslee J. P., Ajhar E. A., Fletcher A. B., Luppino G. A., Metzger M. R., Moore C. B., 2001, ApJ, 546, 681
Tripp R., 1998, A&A, 331, 815
Tully R. B., 1988, ngc..book,
Valentini G., et al., 2003, ApJ, 595, 779
Wang X., et al., 2008, ApJ, 675, 626
Weyant A., Wood-Vasey W. M., Allen L., Garnavich P. M., Jha S. W., Joyce R., Matheson T., 2014, ApJ, 784, 105

Acknowledgements. This research was supported by the DFG cluster of excellence Origin and Structure of the Universe' B.L. acknowledges support for this work by the Deutsche Forschungsgemeinschaft through TRR33, The Dark Universe and the Mount Stromlo Observatory for a Distinguished Visitorship during which most of this publication was prepared.